

# Electron beam induced reduction of $V_2O_5$ studied by analytical electron microscopy

D.S. Su\*, M. Wieske, E. Beckmann, A. Blume, G. Mestl and R. Schlögl

Fritz-Haber-Institut der Max-Planck-Gesellschaft, Abteilung Anorganische Chemie, Faradayweg 4-6, D-14195 Berlin, Germany

Received 2 January 2001; accepted 5 June 2001

The reduction of  $V_2O_5$  under electron irradiation was studied by means of electron energy-loss spectroscopy, electron diffraction, and high-resolution imaging. The decrease of spectral intensity of O 1s excitations indicates a preferential removal of oxygen. The observed chemical shifts of the V 2p<sub>3/2</sub> and V 2p<sub>1/2</sub> peaks reveal that  $V^{5+}$  is reduced to  $V^{2+}$ . Electron diffraction and high-resolution imaging show a structural change from the orthorhombic  $V_2O_5$  to cubic VO. The beam induced reduction is compared with thermal decomposition of  $V_2O_5$ .

**KEY WORDS:**  $V_2O_5$ ; VO; reduction; structural change; electron irradiation; electron microscopy

## 1. Introduction

Vanadium pentoxide,  $V_2O_5$ , is a catalyst widely used in a variety of chemical reactions, *e.g.*, partial oxidation reactions [1] or selective reduction of  $NO_x$  [2]. The interplay between oxygen-bridged  $V^{4+}$  and  $V^{5+}$  ions at the surface of such catalysts is thought to play an important role in these oxidation reactions, namely for the adsorption of oxygen and for its transfer to the organic substrate. However, all of the models proposed for these mechanisms suffer from the fact that the local structure of the active reaction centre is unknown. In the case of selective catalytic reduction, different vanadium phases were reported, namely,  $V_2O_5$ ,  $V_6O_{13}$ , and  $VO_2$ , plus different molecular species. Reliable structural information on vanadium oxides is a prerequisite for unravelling the exact reaction mechanisms of the above mentioned reactions.

In the present work, the phase transition and accompanying reduction of single crystal  $V_2O_5$  by electron irradiation is studied in an analytical transmission electron microscope (TEM). This is a phase transition taking place in a non-chemical ambient (in high-vacuum environment). The knowledge obtained about the reduction under such *simple* conditions could help in our understanding of the reduction mechanism of  $V_2O_5$  in more complicated chemical environments, such as in real catalytic processes. TEM with the facilities of electron energy-loss spectroscopy (EELS) is a powerful tool to characterise catalytic materials; structural changes can be analysed by means of electron diffraction and imaging, while changes in chemical compositions and in oxidation states can be studied by recording EEL spectra followed by analysis of the electron energy-loss near-edge structure (ELNES).

\* To whom correspondence should be addressed.

$V_2O_5$  crystallises with an orthorhombic unit cell, and belongs to the space group  $Pmmn$  [3]. The stereochemistry of vanadium ions in  $V_2O_5$  can be considered to be either distorted trigonal bipyramid, or distorted octahedron [4]. For the distorted octahedral coordination the  $V_2O_5$  crystal structure can be thought of as being built up from edge-sharing and corner-sharing  $VO_6$  octahedra in two levels. The long V–O distance between the levels leads to the formation of a weak interlayer bonding in the [001] direction. Thus, crystalline  $V_2O_5$  exhibits a layered structure with an easily cleaved (001) plane.

## 2. Experimental

$V_2O_5$  crystals were grown by the chemical vapour transport (CVT) technique [5] in a two-zone furnace. The temperature in the two different heating zones was controlled by Eurotherm (Syspro Cal 3200) temperature controllers.  $V_2O_5$  powder was used as the source material. The sealed silica transport tubes used were 15.5 mm in diameter and 170 mm in length. The  $V_2O_5$  powder was loaded at one end of the silica tube. The tube was heated with a flare gun at  $2 \times 10^{-4}$  mbar for *ca.* 15 min to remove adsorbed water and then filled with argon.  $NH_4Cl$  was added (1 mg/ml) [6,7] as the transport agent. Subsequently, the tube was evacuated to  $2 \times 10^{-4}$  mbar and sealed. The loaded transport tube was kept in the horizontal furnace, and after a reverse transport step ( $T_2 = 550^\circ C$ ,  $T_1 = 650^\circ C$ ) for 7 days to purify the sink, the source was endothermically transported ( $T_2 = 600^\circ C$ ,  $T_1 = 500^\circ C$ ) for 28 days. In order to avoid  $NH_4Cl$  condensation on the crystal surfaces, a brief reverse transport step was carried out at the end of the experiment. Subsequently, the transport tubes were slowly cooled down to room temperature and transferred to a glove bag filled with argon in which the tubes were opened. For storage, the

samples were transferred to a glove box (M. Braun, MB150 BGI,  $O_2$  and  $H_2O < 1$  ppm). X-ray diffraction investigations confirmed the orthorhombic structure of the produced  $V_2O_5$  single crystals.

For TEM investigations,  $V_2O_5$  crystals were crushed gently in carbon tetrachloride. Due to the weakly bonded layers mentioned above, most of the crushed pieces were cleaved along the (001) plane and were thin enough for TEM studies. A drop of the solution containing the flakes was placed onto a copper mesh grid covered with a holey carbon film and allowed to dry. All investigations were performed on flakes lying over holes in the carbon film. A Philips CM200 FEG electron microscope, operating at 200 kV and equipped with a GATAN imaging filter GIF100, was used. The high vacuum of the specimen chamber was kept lower than  $10^{-7}$  Torr. The imaging filter, operated in the spectroscopy mode, was used to record EEL spectra. The recorded EEL spectra were corrected for background and multiple scattering [8]. The reduction of  $V_2O_5$  was performed at a current density of  $3 \text{ A/cm}^2$ . The irradiated area was about 5000 nm in diameter and the averaged sample thickness was estimated to be about 140 nm. Electron diffraction patterns were taken before the corresponding EEL spectra were recorded. A TEM heating stage was used for the decomposition of  $V_2O_5$  in high vacuum. The heating rate is  $20^\circ\text{C/min}$ .

### 3. Results

#### 3.1. ELNES

A series of ELNES after different irradiation times is shown in figure 1. The initial spectrum (0 min) is characterised by the vanadium  $2p \rightarrow 3d$  transition (V L-edge) and oxygen  $1s \rightarrow 2p$  transitions (O K-edge): the first two fea-

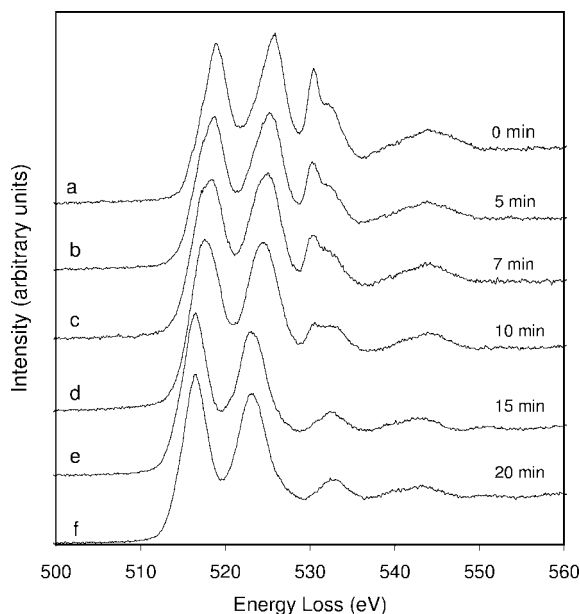


Figure 1. V 2p and O 1s ELNES of  $V_2O_5$  as a function of irradiation time. Spectra are offset for distinction. The electron current density was  $3 \text{ A/cm}^2$ .

tures, located at 519 and 526.7 eV, are attributed to the transitions from the V  $2p_{3/2}$  and V  $2p_{1/2}$  core levels to the unoccupied V 3d bands, respectively. The O K-edge is characterised by the strong hybridisation of the V 3d electrons with the O 2p electrons. The peak at 530.5 eV can be associated to the  $t_{2g}$  component of the V 3d–O 2p orbital-overlapping, and the shoulder at 532.5 eV can be associated to the  $e_g$  component of this overlapping. The feature at 543 eV is related to the transitions from the O 1s core level to the hybridised V 4s–O 2p state.

Irradiation for 5 min already produces changes in these peaks. The spectral intensity of the V  $2p_{1/2}$  peak, as compared to that of the V  $2p_{3/2}$  peak, begins to decrease (spectrum (b)). A fine shoulder appears at 517 eV on the V  $2p_{3/2}$  peak and becomes more pronounced after 7 min irradiation (spectrum (c)). With prolonged irradiation this shoulder shifted slightly to lower energy values, and developed into the peak at 516.5 eV after 20 min irradiation. The original peak at 519 eV disappears. Similar developments can be observed for the V  $2p_{1/2}$  peak which shifted from 526.7 to 523.1 eV after 20 min irradiation. The appearance of the shoulder and the broadening of the V 2p peaks indicate that the spectra (b)–(e) are composed of both unreduced and reduced vanadium cations.

The most significant change in the O K-edge is the decrease of the spectral intensity of the  $t_{2g}$  component at 530 eV until its disappearance after 20 min. The decrease in this intensity is considered to be due to the decrease of the transition probability of the O 1s electron to the first unoccupied hybridisation state between O 2p and V 3d. It has been observed that the intensity of the first unoccupied state decreases as the number of vanadium 3d electrons increases [9]. The shoulder at 532.5 eV due to the  $e_g$  component of the hybridised orbitals developed into a unique peak at 533 eV after 20 min irradiation. The observed changes of the spectral feature at 544 eV are not significant; this may confirm that the upper hybridisation states are not very sensitive to the local symmetry [9]. After 20 min irradiation, further changes in V and O core-level spectra could not be observed.

The chemical shift of the L-edge of 3d transition metal oxides is an indicator of changes in oxidation state of metal atoms in the oxides. In the present work, the peak energy of V  $2p_{3/2}$  is shifted from 519 to 516.5 eV. According to Chen *et al.* [10], in binary vanadium oxides a V  $2p_{3/2}$  peak at 516.5 eV corresponds to the  $V^{2+}$  oxidation state. Our measurement on VO confirms the similarity of spectrum (f) to that of VO.

#### 3.2. Electron diffraction

A series of diffraction patterns, corresponding to the spectra series of figure 1, is given in figure 2. The pattern in figure 2(a) is from  $V_2O_5$  at the very beginning of the irradiation. A structural change could be recognised after 5 min irradiation: additional weak spots appear in the vicinity of 020 reflections (figure 2(b)). As the irradiation time increases,

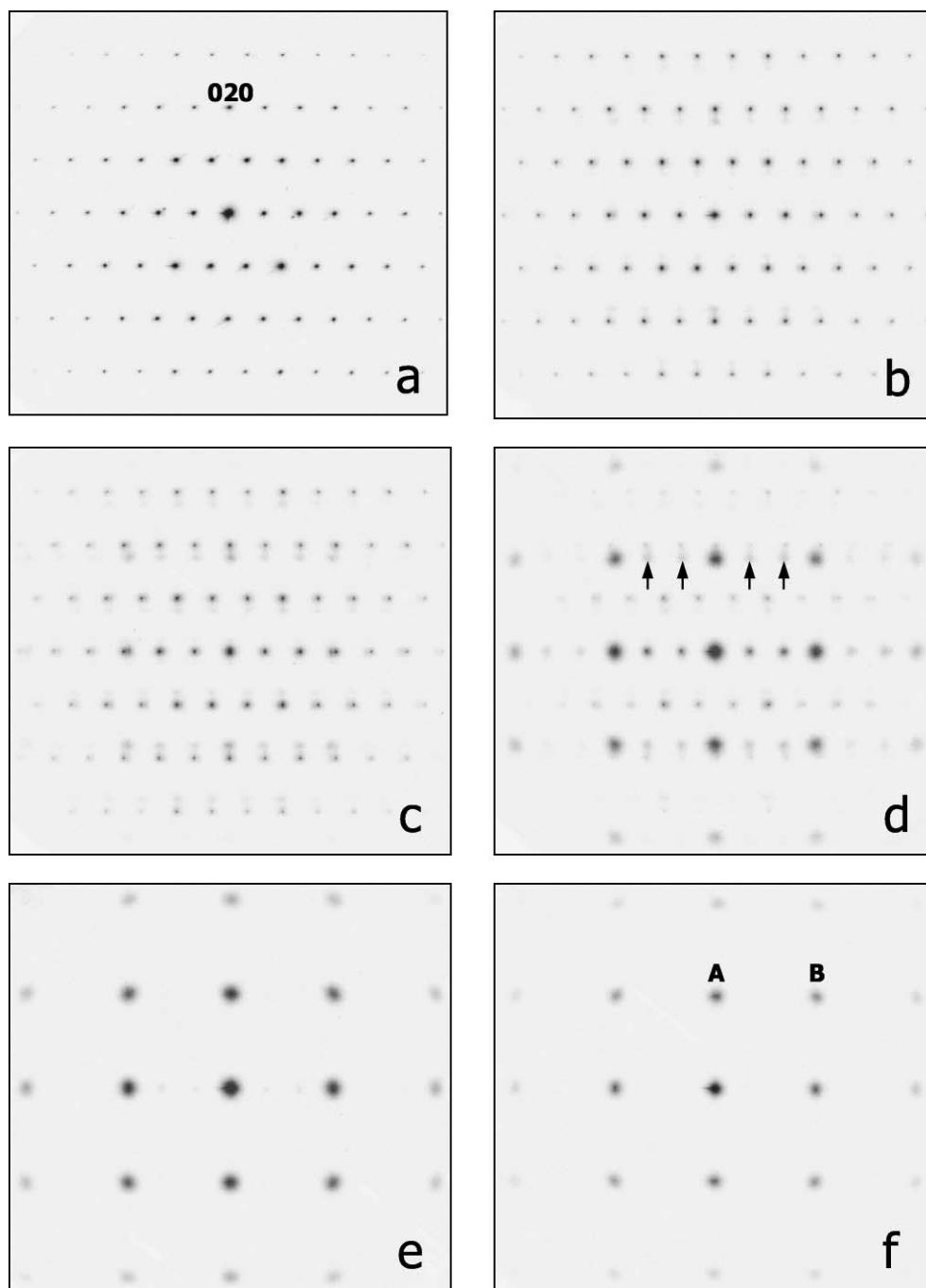


Figure 2. Electron diffraction patterns at irradiation times during which the corresponding energy-loss spectra of figure 1 were recorded. The spots marked by arrows disappear during prolonged irradiation.

more extra spots become visible, forming arrays (figure 2(c)) which are absent in the initial state. After 10 min irradiation, certain extra spots become stronger while the intensities of other extra spots do not change significantly. The diffraction pattern in figure 2(d) shows a tetragonal feature dominated by the strong extra spots, while the spots due to unreduced  $V_2O_5$  are still present. By further irradiation, the weak extra spots marked in pattern 2d disappear; the Bragg spots of the original structure become weaker (figure 2(e)) and finally disappear (figure 2(f)). The diffraction pattern taken after 20 min irradiation (figure 2(f)) is again due to a unique

structure. It is obvious that the diffraction patterns of figure 2 (c) and (d) contain Bragg spots from an intermediate phase, which is formed and disappears again during the reduction process. This will be discussed in detail later.

The diffraction pattern from the original  $V_2O_5$  crystal provides a reference calibration for an accurate measurement of the spots in figure 2(f). The reciprocal distances of reflection A and B were measured to be  $4.88$  and  $6.96 \text{ nm}^{-1}$ , respectively. In other words, these spots were measured to have lattice spacings of  $0.205$  and  $0.144 \text{ nm}$ .  $VO_2$ ,  $V_2O_3$ , and  $VO$  were checked as possible structures giving rise to

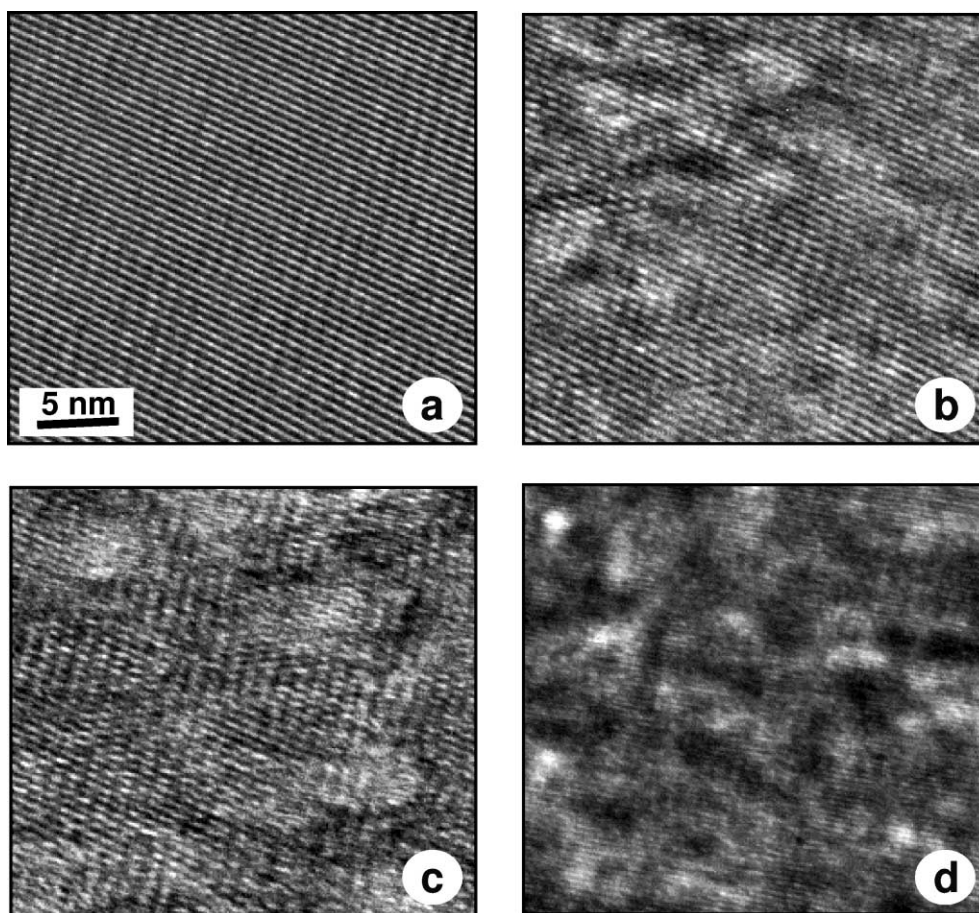


Figure 3. High-resolution images of  $V_2O_5$  during irradiation. Irradiation times: (a) 0, (b) 7, (c) 10, and (d) 15 min. The  $V_2O_5$  specimen is oriented slightly off the 001 axis.

the patterns. Among them, only VO of cubic structure has similar lattice parameters  $d_{020} = 0.206$  nm and  $d_{220} = 0.146$  nm, respectively. The calculated lattice parameter of  $a = b = 0.410$  nm is in good agreement with the lattice parameter of VO (0.412 nm). Hence, it can be concluded that VO is the structure which results from the reduction of  $V_2O_5$  by the electron irradiation in the microscope.

Note that in the diffraction pattern series in figure 2 the additional spots do not appear randomly. This means that the formation of the intermediate phase and of VO proceeds well-oriented with respect to  $V_2O_5$ . The indexing of the pattern in figure 2(f) reveals that the final product VO grows with the [001] axis parallel to the  $a$ -axis of  $V_2O_5$  and with the [010] axis parallel to the  $b$ -axis.

### 3.3. High-resolution TEM

A series of high-resolution images recorded during beam irradiation is reproduced in figure 3, and show the alternation of lattice fringes of the irradiated area. The sample is nearly (001) oriented. Figure 3(a) shows the 110-lattice fringes of  $V_2O_5$  recorded at the very beginning of irradiation. Irradiation causes changes in contrast, resulting in faint and diffuse lattice fringes (figure 3(b)). A careful study of image (c) reveals lattice fringes with different spacing. This bears evi-

dence of the co-existence of different phases at this reduction stage, as already deduced from the diffraction patterns. The lattice fringes shown in figure 3(d) are measured to have a spacing of 0.20 nm, *i.e.*, they are from the 200-planes of VO. This again confirms that the final reduced product is VO. The images in figure 3 (b) and (c) indicate that the reduction of  $V_2O_5$  did not follow layer by layer. Islands of reduced materials are formed first and spread out over the irradiated area after 15 min. Note that the lattice fringes of the final reduced area in figure 3(d) look like those of a single crystal, implying that all of the islands initially formed grow well-oriented on  $V_2O_5$  until its complete reduction.

## 4. Discussion

The important results of the present work are: (i)  $V_2O_5$  can be reduced to VO in high vacuum by electron irradiation; (ii) intermediate phases and the final product have a well-defined orientation relationship to the original  $V_2O_5$ ; (iii) the reduction seems to begin at individual points where islands of the intermediate phase grow. This is different from the general assumption that the reduction occurs at the surface and develops then layer by layer.

Figure 4 shows a series of ELNES of  $V_2O_5$  recorded during a thermal decomposition experiment on a heating

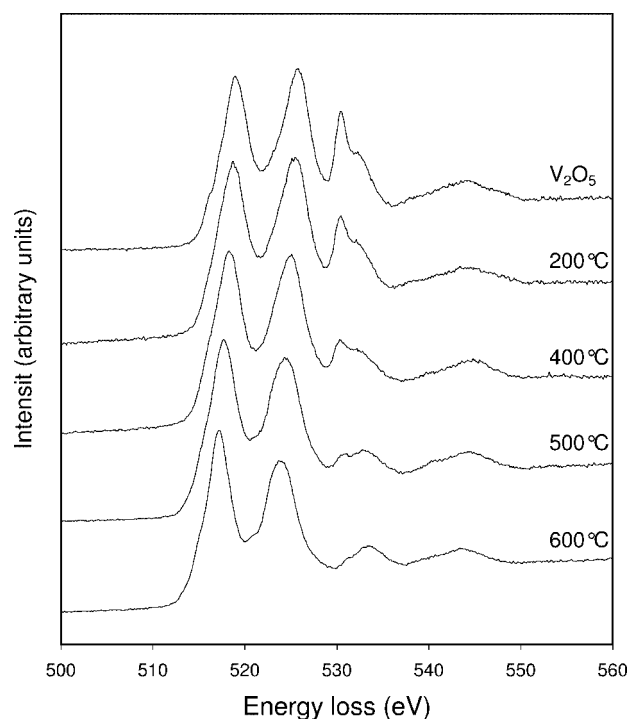


Figure 4. V 2p and O 1s ELNES of  $V_2O_5$  recorded at various temperatures. Spectra are offset for distinction. The heating rate was 20 °C/min.

stage in a Philips CM200 FEG electron microscope. At first glance the changes occurring in the spectra in figures 1 and 4, as the reduction develops, are quite similar. However, detailed studies of the thermal decomposition (that will be published elsewhere) reveal that  $V_2O_5$  transforms to  $V_2O_3$  at 600 °C, via the  $VO_2$  phase that formed at 400 °C. This finding is in agreement with earlier reports on annealing  $V_2O_5$  from 200 to 600 °C [11,12], but differs from the electron-beam induced reduction.

The well-accepted mechanism of the reduction of  $V_2O_5$  to  $V_6O_{13}$  is the loss of oxygen atoms from every third (010) plane and a crystallographic shear in the [001] direction [4]. Recently, it has been suggested that  $V_6O_{13}$  can be further transformed to  $VO_2$  by the same mechanism [13]. The reduction of  $V_2O_5$  to  $V_6O_{13}$  can then be described by the loss of oxygen from the top V–O layer of  $V_2O_5$  in the first stage followed by the diffusion of oxygen from the bulk to the surface so that the oxygen concentration of the top layer is replenished to the requirements of the corresponding lattice of  $V_6O_{13}$  [7,12]. Such preferential loss of oxygen atoms at the surface of metal oxides can be induced by an inter-atomic Auger process excited by incident electrons [14]. The high-resolution images shown in figure 3 indicate that under the electron beam, reduction starts over the entire irradiated area; however, small islands are formed in which the reduction occurs faster. Such islands, well-oriented on the surface as well as in the bulk of  $V_2O_5$ , were the first reduced to VO and subsequently spread out until the whole irradiated area was reduced to VO. Therefore, the mechanism of reduction induced by electron beam differs from the conventional layer-by-layer reduction mechanism.

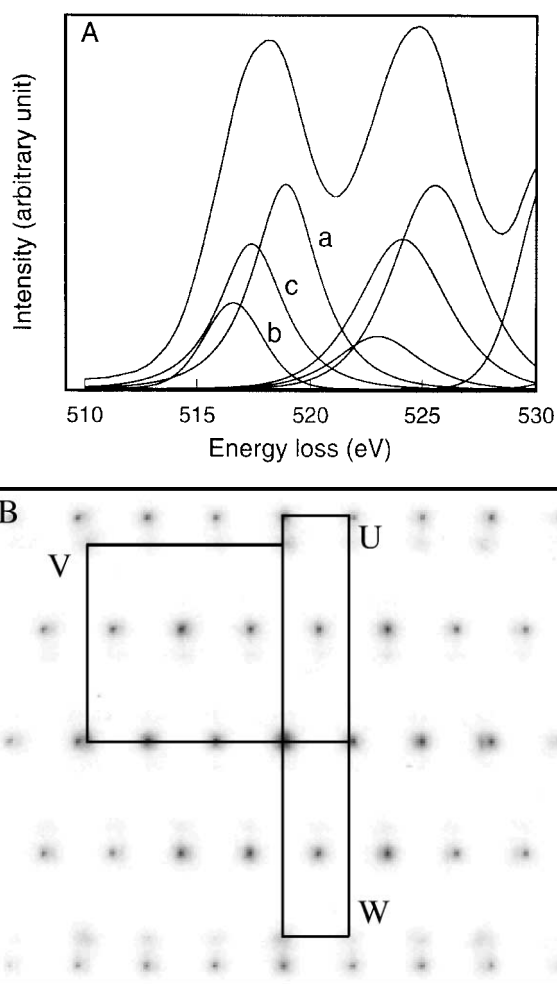


Figure 5. (A) V 2p ELNES after 7 min irradiation. The V  $2p_{3/2}$  peak can be fitted as a sum of two Gauss curves (a) for  $V_2O_5$  (max. at 519 eV) and (b) for VO (max. at 516.5 eV) resulting in (c) (max. at 517.5 eV) for the intermediate phase. (B) Electron diffraction pattern after 7 min irradiation. The reciprocal unit cells of the  $V_2O_5$ , VO, and the intermediate phase are indicated by U, V, and W, respectively.

The apparently different reduction mechanisms can be due to the fact that the interaction of the electron beam with samples is more complex than just the increasing of the bulk temperature. Since we also observed the electron beam induced reduction of  $V_2O_5$  in a cryo-electron microscope keeping at 4 K, the reduction could be caused by a radiolysis process [15]: inelastic scattering of electrons breaks chemical bonds of oxygen and vanadium thus changing the specimen's chemistry and the structure of the bulk through a series of reactions driven by the electron beam. Radiolysis can preferably take place at point or planar defects or impurities where dangling bonds or weakly bonded atoms exist. This could be the explanation why islands were firstly formed on  $V_2O_5$  during the reduction, as observed by high-resolution imaging.

It is interesting to find out if the reduction process shown in figures 1 and 4 have the same intermediate phases. In figure 5(A) the V 2p ELNES obtained after 7 min irradiation was decomposed into components matching the V 2p

ELNES of  $V_2O_5$ , VO, and an intermediate phase with the energy position of the V 2p<sub>3/2</sub> peak at 517.5 eV. This energy value is very close to the V 2p<sub>3/2</sub> peak of  $V_2O_3$  at 517.4 eV. According to Chen *et al.* [10], the detected phase should be a compound between  $VO_2$  and  $V_2O_3$ , containing vanadium  $V^{4+}$  and  $V^{3+}$  ions. Figure 5(B) shows that the diffraction pattern, also taken after 7 min irradiation time, is a superposition of the three patterns from  $V_2O_5$ , VO, and the intermediate phase. Among all the known phases with oxidation state similar to  $V_2O_3$ , we cannot find any whose reciprocal unit cell can be identified with the one shown in figure 5(B).  $V_4O_9$  and a modified  $V_6O_{13}$  were observed as intermediate phases in reductions of vanadium pentoxide under the high-energy electron beam irradiation in an electron microscope [16]. However, the positions of V 2p peaks from these two phases are much higher than the V 2p peak position of the intermediate phase detected in the present work.

The reported observation of the structural instability of high oxidation state vanadium oxides is highly relevant for catalyst characterisations by HRTEM and other UHV methods, like LEED or XPS. The observed extreme reduction to even VO within only 20 min irradiation indicates how critical it is to control the conditions (*i.e.*, atmosphere, temperature) during the structural characterisation of catalytically active oxides. Our results suggest that several pathways are necessary to explain the structural transformations of  $V_2O_5$  during reduction since the sequence of phase transitions depends strongly on thermal, chemical, and external experimental (electron-beam) conditions.

## 5. Summary

Analytical TEM was used to characterise the reduction of 001-oriented  $V_2O_5$  crystals by electron irradiation in an electron microscope. The decrease of oxygen 1s signals suggested a preferential loss of oxygen. The chemical shift of V 2p<sub>3/2</sub> peaks from 519 to 516.5 eV indicated that  $V^{5+}$  is reduced even to  $V^{2+}$ . Electron diffraction patterns reveal that

the final reduced state was (001)-oriented cubic VO. High-resolution images show that the irradiation forms islands of reduced materials on  $V_2O_5$ . An intermediate phase containing  $V^{3+}$  and  $V^{2+}$  ions has been suggested. The electron beam induced reduction pathway differs from that of thermal decomposition.

## Acknowledgement

The work is supported by SFB 546 of the Deutsche Forschungsgemeinschaft (DFG).

## References

- [1] J. Haber, in: *Handbook of Heterogeneous Catalysis*, Vol. 4, eds. G. Ertl, H. Knözinger and J. Weitkamp (Wiley-VCH, Weinheim, 1997) p. 2253.
- [2] F.J. Janssen, in: *Handbook of Heterogeneous Catalysis*, Vol. 4, eds. G. Ertl, H. Knözinger and J. Weitkamp (Wiley-VCH, Weinheim, 1997) p. 1633.
- [3] H.G. Bachmann, F.R. Achmed and W.H. Barness, *Z. Kristallogr.* 115 (1961) 110.
- [4] H. Haber, M. Witko and R. Tokarz, *Appl. Catal. A* 157 (1997) 3.
- [5] H. Schäfer, *Chemische Transportreaktionen* (Verlag Chemie, Berlin, 1962).
- [6] M. Wenzel and R. Gruehn, *Z. Anorg. Allg. Chem.* 582 (1990) 75.
- [7] M. Wenzel and R. Gruehn, *Z. Anorg. Allg. Chem.* 568 (1989) 95.
- [8] R. Egerton, *Electron Energy-Loss Spectroscopy in the Electron Microscope* (Plenum, New York, 1996).
- [9] X.W. Lin, Y.Y. Wang, V.P. Dravid, P.M. Michalakos and M.C. Kung, *Phys. Rev. B* 47 (1993) 3477.
- [10] J.G. Chen, C.M. Kim, B. Frühberger, B.D. De Vries and M.S. Touvelle, *Surf. Sci.* 321 (1994) 145.
- [11] J.B. MacChesney, J.F. Potter and H.J. Guggenheim, *J. Electrochem. Soc.* 115 (1968) 52.
- [12] E. Gillis, *Compte Rend. Acad. Sci. Paris* 258 (1964) 4765.
- [13] H. Katzke *et al.*, to be published.
- [14] N.H. Tolk, M.M. Traum, J.C. Tully and T.E. Madley, eds., *Desorption Induced by Electronic Transitions, DIET I* (Springer, Berlin 1983).
- [15] L. Hobbs, in: *Introduction to Analytical Electron Microscopy*, ed. J. Hren (Plenum, New York, 1979) p. 437.
- [16] H.J. Fan and L.D. Marks, *Ultramicroscopy* 31 (1989) 357.